ISSN 0304-9892 (Print) ISSN 2455-7463 (Online)
www.vijnanaparishadofindia.org/jnanabha
***Jñānābha*, Vol. 52(2) (2022), 237-249**
*(Dedicated to Professor D. S. Hooda on His* $80^{th}$ *Birth Anniversary Celebrations)*

# INVESTIGATION OF MASS TRANSFER PHENOMENON IN BIOMAGNETIC FLUID FLOW UNDER STENOTIC CONDITION

**Subrata Mukhopadhyay**
Department of Mathematics, Acharya P. C. Roy Government College, Siliguri-734010, West Bengal, India
Email: subratamath@yahoo.in

*(Received: February* 04*,* 2022*; Revised: May* 20*,* 2022*; Accepted: November* 16*,* 2022*)*

DOI: https://doi.org/10.58250/jnanabha.2022.52228

**Abstract**

Initiation and development of atherosclerosis are closely related to the mass transfer mechanism of blood constituents onto the arterial wall. Investigation of mass transfer phenomenon in magnetohydrodynamic ( *MHD*) flow of blood through a stenosed artery is the objective of this study. Carreau viscosity model is used to describe the non-Newtonian character of streaming blood. Vessel wall flexibility is taken into account. Pulsatile flow of blood is governed by the Navier-Stokes equations along with the mass conservation equation. Mass transfer phenomenon is governed by the convection-diffusion equation coupled with the velocity field. A finite difference scheme is developed and suitable initial and boundary conditions are imposed to solve these non-linear equations. Distributions of several significant wall parameters, such as time-averaged wall shear stress, time-averaged Sherwood number etc. are examined over the entire flow regime with the variations of stenosis height, Hartmann number and Schmidt number. Comparison with the Newtonian fluid for these wall parameters are done. Patterns of stream lines and iso-concentration lines are also shown for additional qualitative insight of the flow-field and concentration-field.

**2020 Mathematical Sciences Classification:** 76A05, 76W05, 76Z05.
**Keywords and Phrases:** *MHD* flow; mass transfer; non-Newtonian fluid; pulsatile flow; stenosed artery.

## 1. Introduction

Analytical and experimental investigations of arterial blood flow under stenotic condition have become an interesting field of research during last few decades because of the fact that cardiovascular diseases are now a major cause of mortality worldwide. Partial occlusion within an arterial wall due to formation of fibrous and fatty plaques is known as an arterial stenosis which restricts the normal flow of blood to the distal bed. Dynamics of arterial blood flow is believed to play a significant role in the genesis and development of atherosclerosis. Thus study of hemodynamics past an arterial stenosis bears a good aspect due to its feasible medical application.

Experimental observations reveal that blood, being a complex suspension of cells, behaves like a non-Newtonian fluid at low shear rates in tubes of small diameters [3,8,29]. There are quite a good number of experimental as well as theoretical research works related to the hemodynamics of blood flow through stenosed arteries ([9],[14],[16],[18],[19],[21],[25]). But in most of these studies either the vascular wall deformability or the pulsatile nature of blood flow has been disregarded.

Although, commencement and propagation of atherosclerotic plaques are often found associated with low and oscillatory shear stress at arterial wall [11], some researchers reported that such constrictions may not be the effect of only wall shear stress. According to Caro et al. [2], atherosclerotic lessons may develop due to the mass transfer mechanism between streaming blood and the vessel wall. Several researchers [1,10,13,17,22,23,30] have investigated the mass transfer phenomenon in unsteady flow of blood through constricted arteries. But in these studies either the flow profile is not physiological or the vessel wall is considered to be rigid.

Recently the study of magnetohydrodynamics (*MHD*) of arterial blood flow has become important due to its several significant clinical implications. Examples include the studies of magnetic drug targeting [28] and the development of magnetic devices for cell separation [7]. A good number of research works can be found in open literature where magnetohydrodynamics of blood flow through diseased arteries has been investigated [15,24,26,27].

The purpose of the present theoretical work is to investigate the influence of the externally imposed magnetic field on the mass transfer mechanism of blood flowing through a stenosed artery. Non-Newtonian behaviour of blood viscosity, flexibility of arterial wall, physiologically realistic pulsatile flow of blood all are taken into account to represent the actual arterial flow. The arterial segment is assumed to be a cylindrical straight tube with deformable wall geometry. Complete Navier-Stokes equations in cylindrical coordinates governing pulsatile flow of blood and the mass transport equation coupled with the velocity field in dimensionless form are taken up along with suitable initial and boundary conditions and are solved using the stream function-vorticity approach.

## 2. Blood Viscosity Model

Experimental results reveal that human blood exhibits non-Newtonian character in small diameter arteries and its viscosity is shear thinning. Selection of an appropriate non-Newtonian model for blood viscosity is essential to achieve acceptable results. Carreau viscosity model is a good approximation to non-Newtonian viscosity of blood at low shear rates which behaves like a Newtonian model at high shear rates [25].

The Carreau viscosity model for human blood is described as:

$$\mu^*(\dot{\gamma}^*) = \mu_\infty + (\mu_0 - \mu_\infty)(1 + \Lambda^{*2}\dot{\gamma}^*)^{(n-1)/2}, \tag{2.1}$$

where $\dot{\gamma}^*$ is the shear rate, $\mu_0$ and $\mu_\infty$ are the asymptotic zero and infinite shear viscosities, $\Lambda^* \geq 0$ is a material constant that represents the degree of shear thinning. Values of these parameters for human blood are $\mu_0 = 0.056Pas, \mu_\infty = 0.00345Pas, \Lambda^* = 3.313s, n = 0.3568$ [4].

## 3. Governing equations

Two-dimensional laminar and pulsatile flow of an electrically conducting incompressible viscous non-Newtonian fluid with electrical conductivity $\sigma$ and constant density $\rho$ flowing through an axi-symmetric straight tube (modeled as an artery) having a bell-shaped axi-symmetric constriction is taken. Cylindrical polar coordinates $(r^*, \theta^*, z^*)$ are used and the arterial axis is taken as the $z$-axis. $z^* = 0$ represents the inlet cross section. Let $R^*(z^*, t^*)$ be the radius of the artery at time $t^*$and $R_0 = R^*(0, 0)$. Also, let $p^*$ be the pressure, $u^*$ and $v^*$ be the axial and radial components of velocity respectively. Axial symmetry makes all these variables independent of $\theta^*$.

A uniform magnetic field $B_0$ is considered in the transverse direction. The magnetic permeability of the conducting medium is assumed to be constant.

Following non-dimensional variables are now introduced

$$z = \frac{z^*}{R_0}, r = \frac{r^*}{R_0}, R = \frac{R^*}{R_0}, u = \frac{u^*}{U_0}, v = \frac{v^*}{U_0}, t = \frac{t^*}{T}, p = \frac{p^*}{\rho U_0^2},$$
$$\mu = \frac{\mu^*}{\mu_\infty}, \lambda = \frac{\mu_0}{\mu_\infty}, \Lambda = \frac{\Lambda^* U_0}{R_0}, \dot{\gamma} = \frac{\dot{\gamma}^* R_0}{U_0}, \tag{3.1}$$

where $U_0$ is the characteristic flow velocity and $T$ is the period of the flow pulsation.

The Navier-Stokes equations for a homogeneous viscous incompressible fluid may be put in dimensionless form as

$$St\frac{\partial u}{\partial t} + \frac{\partial(uv)}{\partial r} + \frac{\partial(u^2)}{\partial z} + \frac{uv}{r} = -\frac{\partial p}{\partial z} + \frac{1}{Re}[\mu(\frac{\partial^2 u}{\partial r^2} + \frac{1}{r}\frac{\partial u}{\partial r} + \frac{\partial^2 u}{\partial z^2})$$
$$(+\frac{\partial \mu}{\partial r}(\frac{\partial u}{\partial r} + \frac{\partial v}{\partial z}) + 2\frac{\partial \mu}{\partial z}\frac{\partial u}{\partial z}] - \frac{Ha^2}{Re}u \tag{3.2}$$

and

$$St\frac{\partial v}{\partial t} + \frac{\partial(v^2)}{\partial r} + \frac{\partial(uv)}{\partial z} + \frac{v^2}{r} = -\frac{\partial p}{\partial r} + \frac{1}{Re}[\mu(\frac{\partial^2 v}{\partial r^2} + \frac{1}{r}\frac{\partial v}{\partial r} + \frac{\partial^2 v}{\partial z^2} - \frac{v}{r^2})$$
$$(+2\frac{\partial \mu}{\partial r}\frac{\partial v}{\partial r} + \frac{\partial \mu}{\partial z}(\frac{\partial v}{\partial z} + \frac{\partial u}{\partial r})] \tag{3.3}$$

Also the mass conservation equation is

$$r\frac{\partial u}{\partial z} + \frac{\partial(vr)}{\partial r} = 0. \tag{3.4}$$

$Re = U_0 R_0 \rho/\mu_\infty$, $St = R_0/(U_0 T)$ and $Ha = B_0\sqrt{\frac{\sigma R_0}{U_0 \rho}}$ being the flow Reynolds number, Strouhal number and Hartmann number respectively.

The mass transport mechanism in the blood stream is governed by the non-dimensional equation

$$St\frac{\partial C}{\partial t} + u\frac{\partial C}{\partial z} + v\frac{\partial C}{\partial r} = \frac{1}{ReSc}[\frac{\partial^2 C}{\partial r^2} + \frac{1}{r}\frac{\partial C}{\partial r} + \frac{\partial^2 C}{\partial z^2}]. \tag{3.5}$$

Here, $Sc = \frac{\mu}{\rho D}$ is the Schmidt number, $D$ being the coefficient of diffusion.

The dimensionless blood viscosity is obtained as

$$\mu(\dot{\gamma}) = 1 + (\lambda - 1)\{1 + \Lambda^2\dot{\gamma}\}^{(n-1)/2} \tag{3.6}$$

with

$$\dot{\gamma} = [2(\frac{\partial u}{\partial z})^2 + 2(\frac{\partial v}{\partial r})^2 + 2(\frac{v}{r})^2 + (\frac{\partial u}{\partial r} + \frac{\partial v}{\partial z})^2]^{\frac{1}{2}}.$$

A dimensionless physiological pulsatile flow rate proposed by Pedrizzetti [20]

$$fr(t) = 0.4355 + 0.05\cos 2\pi t + 0.25\sin 2\pi t - 0.13\cos 4\pi t + 0.13\sin 4\pi t - 0.10\cos 6\pi t - 0.02\sin 6\pi t - 0.01\cos 8\pi t - 0.03\sin 8\pi t \quad (3.7)$$

is assumed through the tube. Systolic and diastolic peak flow times of this flow profile are $t = 0.18$ and $t = 0.45$ respectively (Fig. 3.1).

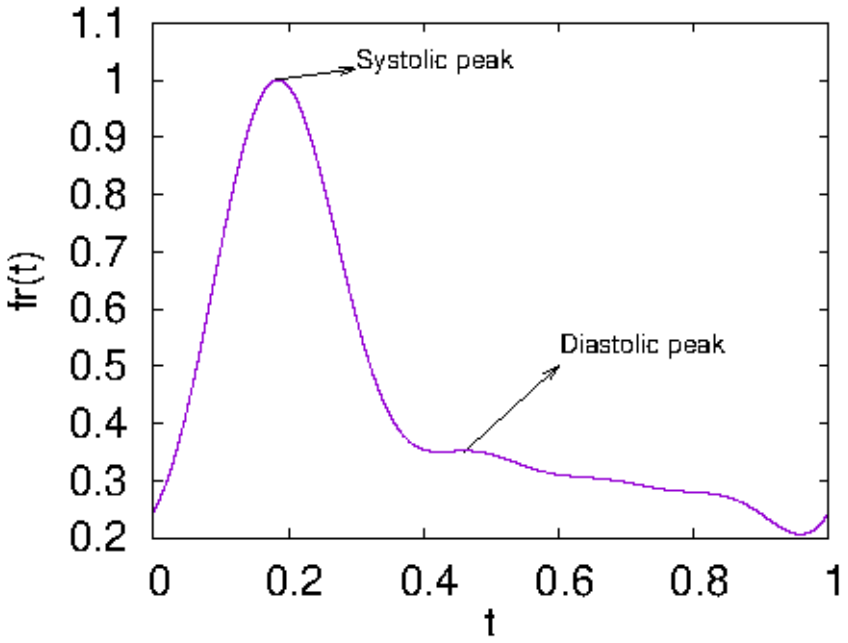


***Figure* 3.1:** Pulsatile flow rate proposed by Pedrizzetti [20].

## 4. Geometry of the tube

The wall geometry of the arterial segment under consideration at $t = 0$ may be represented in non-dimensional form as:

$$R(z, 0) = [1 - \delta e^{-\sigma(z-a)^2}]a(t), 0 \le z \le L, \quad (4.1)$$

where $a$ and $\delta$ describe the position and height of the stenosis, $\sigma$ represents the rate at which the boundary profile changes and $L$ is the length of the flow regime under consideration.

As the wall deformation must be proportional to the flow rate, the time-variant parameter $a_1(t)$ is chosen as [16]

$$a(t) = 1 + k\{fr(t) - fr(0)\} \quad (4.2)$$

where $k$ is the amplitude parameter and $fr(t)$ is the pulsatileflow rate.

Schematic diagram of the artery is presented in Fig . 4.1. The parameter values $\sigma = 5, a = 3.5, L = 10, k = 0.01$ is taken in this study.

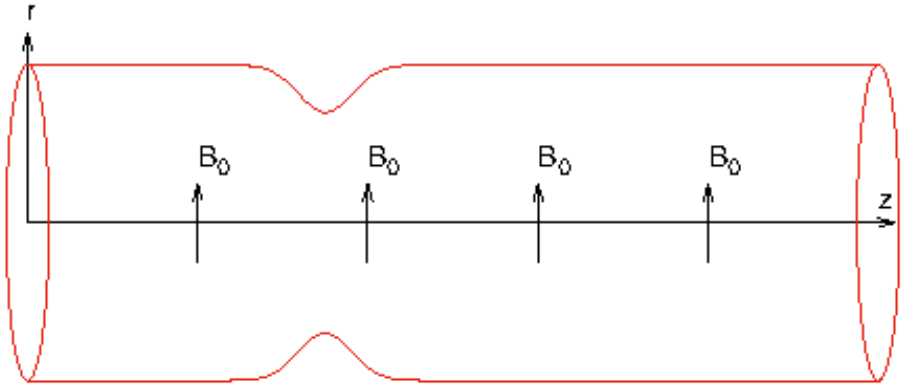


***Figure* 4.1:** Schematic diagram of the stenosed flexible artery at time $t = 0$.

## 5. Stream function-Vorticity formulation

The dimensionless stream function $\psi(z, r, t)$ is defined by

$$u = \frac{1}{r}\frac{\partial \psi}{\partial r}, v = -\frac{1}{r}\frac{\partial \psi}{\partial z} \tag{5.1}$$

and the corresponding vorticity function $\omega(z, r, t)$ by

$$\omega = \frac{\partial v}{\partial z} - \frac{\partial u}{\partial r}. \tag{5.2}$$

The pressure derivative terms in the momentum Eqs. (3.2) and (3.3) are now eliminated by cross-differentiation. The vorticity transport equation is obtained as

$$St\frac{\partial \omega}{\partial t} + u\frac{\partial \omega}{\partial z} + v\frac{\partial \omega}{\partial r} - \frac{v\omega}{r} = \frac{1}{Re}[\mu(\frac{\partial^2 \omega}{\partial z^2} + \frac{\partial^2 \omega}{\partial r^2} + \frac{1}{r}\frac{\partial \omega}{\partial r} - \frac{\omega}{r^2}) + 2\frac{\partial \mu}{\partial z}\frac{\partial \omega}{\partial z} + \frac{\partial \mu}{\partial r}(2\frac{\partial \omega}{\partial r} + \frac{\omega}{r}) - 2\frac{\partial^2 \mu}{\partial r \partial z}(\frac{v}{r} + 2\frac{\partial u}{\partial z})(+(\frac{\partial^2 \mu}{\partial z^2} - \frac{\partial^2 \mu}{\partial r^2})(\frac{\partial u}{\partial r} + \frac{\partial v}{\partial z})] + \frac{Ha^2}{Re}\frac{\partial u}{\partial r}. \tag{5.3}$$

Also, the continuity equation transforms to the pressure Poisson equation

$$\frac{\partial^2 \psi}{\partial z^2} + \frac{\partial^2 \psi}{\partial r^2} - \frac{1}{r}\frac{\partial \psi}{\partial r} = -\omega r. \tag{5.4}$$

## 6. Initial and Boundary Conditions

The initial conditions for the velocity and concentration field are set as [17]

$$u = \frac{2fr(0)}{\pi R^2}\{1 - (\frac{r}{R})^2\}, v = 0, C = 1 - (\frac{r}{R})^2. \tag{6.1}$$

It is verified that the initial conditions do not affect the final results when the simulation is run for sufficiently long time. It is also found that all transitional effects vanish and the final results do not alter significantly when the simulation is carried out more than three time periods.

For the boundary condition at the inlet cross section of the tube, the flow is assumed to be fully developed i.e.

$$\frac{\partial \omega}{\partial z} = \frac{\partial \psi}{\partial z} = 0 \text{ at } z = 0 \tag{6.2}$$

and at the outlet cross section, the flow field is assumed to have no change which gives

$$\frac{\partial^2 \omega}{\partial z^2} = \frac{\partial^2 \psi}{\partial z^2} = 0 \text{ at } z = L. \tag{6.3}$$

The symmetry of flow field gives

$$\psi = 0, \omega = 0 \text{ along } r = 0. \tag{6.4}$$

At the tube wall the usual 'no-slip' condition is imposed, which gives

$$\frac{\partial \psi}{\partial r} = 0 \text{ along } r = R(z, t). \tag{6.5}$$

Tube wall deformability gives

$$\frac{\partial \psi}{\partial z} = -R\frac{\partial R}{\partial t} \text{ along } r = R(z,t). \tag{6.6}$$

The imposed axial symmetry of the concentration field gives

$$\frac{\partial C}{\partial r} = 0 \text{ along } r = 0. \tag{6.7}$$

A constant concentration of the solute is taken at the inlet while at the outlet the concentration gradient is assumed to be zero. Thus

$$C = 1 \text{ at } z = 0 \text{ and } \frac{\partial C}{\partial z} = 0 \text{ at } z = L. \tag{6.8}$$

A zero concentration on the vessel wall is set as

$$C = 0 \text{ at } r = R(z,t) \tag{6.9}$$

which essentially ignores any coupling between the blood-side and wall-side mass transfer processes and can be used as a first approximation [6].

Now the flow rate across any cross-section is

$$\int_0^{R(z,t)} 2\pi r(\frac{1}{r}\frac{\partial \psi}{\partial r})dr = Q(z,t).$$

This gives the stream function $\Psi$ at the wall as

$$\psi(z, R(z,t), t) = \frac{1}{2\pi}Q(z,t). \tag{6.10}$$

## 7. Coordinate transformation

A suitable radial coordinate transformation [12]

$$x = \frac{r}{R(z,t)}, \tag{7.1}$$

is now employed which maps the constricted region into a rectangular one. This transforms the vorticity transport Eq. (5.3) into

$$\begin{aligned}
&St(\frac{\partial \omega}{\partial t} - \frac{x}{R}\frac{\partial R}{\partial t}\frac{\partial \omega}{\partial x}) + u(\frac{\partial \omega}{\partial z} - \frac{x}{R}\frac{\partial R}{\partial z}\frac{\partial \omega}{\partial x}) + \frac{v}{R}\frac{\partial \omega}{\partial x} - \frac{v\omega}{xR} \\
&= \frac{1}{Re}[\mu\{\frac{\partial^2 \omega}{\partial z^2} + (\frac{x^2}{R^2}(\frac{\partial R}{\partial z})^2 + \frac{1}{R^2})\frac{\partial^2 \omega}{\partial x^2} - \frac{2x}{R}\frac{\partial R}{\partial z}\frac{\partial^2 \omega}{\partial x \partial z} + (\frac{2x}{R^2}(\frac{\partial R}{\partial z})^2 - \frac{x}{R}\frac{\partial^2 R}{\partial z^2} + \frac{1}{xR^2})\frac{\partial \omega}{\partial x} - \frac{\omega}{x^2R^2}\} \\
&+ 2(\frac{\partial \mu}{\partial z} - \frac{x}{R}\frac{\partial R}{\partial z}\frac{\partial \mu}{\partial x})(\frac{\partial \omega}{\partial z} - \frac{x}{R}\frac{\partial R}{\partial z}\frac{\partial \omega}{\partial x}) + \frac{1}{R}\frac{\partial \mu}{\partial x}(\frac{2}{R}\frac{\partial \omega}{\partial x} + \frac{\omega}{xR}) \\
&- \frac{2}{R}(\frac{\partial^2 \mu}{\partial x \partial z} - \frac{1}{R}\frac{\partial R}{\partial z}\frac{\partial \mu}{\partial x} - \frac{x}{R}\frac{\partial R}{\partial z}\frac{\partial^2 \mu}{\partial x^2})(\frac{v}{xR} + 2\frac{\partial u}{\partial z} - \frac{2x}{R}\frac{\partial R}{\partial z}\frac{\partial u}{\partial x}) \\
&+ \{\frac{\partial^2 \mu}{\partial z^2} + (\frac{x^2}{R^2}(\frac{\partial R}{\partial z})^2 - \frac{1}{R^2})\frac{\partial^2 \mu}{\partial x^2} - \frac{2x}{R}\frac{\partial R}{\partial z}\frac{\partial^2 \mu}{\partial x \partial z} + (\frac{2x}{R^2}(\frac{\partial R}{\partial z})^2 - \frac{x}{R}\frac{\partial^2 R}{\partial z^2})\frac{\partial \mu}{\partial x}\}((\frac{1}{R}\frac{\partial u}{\partial x} + \frac{\partial v}{\partial z} - \frac{x}{R}\frac{\partial R}{\partial z}\frac{\partial v}{\partial x})] + \frac{Ha^2}{Re}\frac{1}{R}\frac{\partial u}{\partial x}.
\end{aligned} \tag{7.2}$$

Relation between vorticity and stream function becomes

$$\frac{\partial^2 \psi}{\partial z^2} + \{\frac{x^2}{R^2}(\frac{\partial R}{\partial z})^2 + \frac{1}{R^2}\}\frac{\partial^2 \psi}{\partial x^2} - \frac{2x}{R}\frac{\partial R}{\partial z}\frac{\partial^2 \psi}{\partial x \partial z} + \{\frac{2x}{R^2}(\frac{\partial R}{\partial z})^2 - \frac{x}{R}\frac{\partial^2 R}{\partial z^2} - \frac{1}{xR^2}\}\frac{\partial \psi}{\partial x} = -Rx\omega. \tag{7.3}$$

Value of the stream function at the boundary is

$$\psi(z, x = 1, t) = \frac{1}{2\pi}Q(z,t). \tag{7.4}$$

Making use of Eq. (7.3), the boundary condition for $\omega$ at $x = 1$, is obtained as

$$\omega(z, x = 1, t) = -\frac{1}{R^3}[1 + (\frac{\partial R}{\partial z})^2](\frac{\partial^2 \psi}{\partial x^2})_{x=1} + (\frac{\partial^2 R}{\partial z \partial t} + \frac{1}{R}\frac{\partial R}{\partial z}\frac{\partial R}{\partial t}). \tag{7.5}$$

The transformed form of the mass transport Eq. (3.5) is given by

$$\begin{aligned}
St(\frac{\partial C}{\partial t} - \frac{x}{R}\frac{\partial R}{\partial t}\frac{\partial C}{\partial x}) + u(\frac{\partial C}{\partial z} - \frac{x}{R}\frac{\partial R}{\partial z}\frac{\partial C}{\partial x}) + \frac{v}{R}\frac{\partial C}{\partial x} = \frac{1}{ReSc}[\frac{1}{R^2}\frac{\partial^2 C}{\partial x^2} + \frac{1}{xR^2}\frac{\partial C}{\partial x} + \{\frac{\partial^2 C}{\partial z^2} + \frac{x^2}{R^2}(\frac{\partial R}{\partial z})^2\frac{\partial^2 C}{\partial x^2} - \frac{2x}{R}\frac{\partial R}{\partial z}\frac{\partial^2 C}{\partial x \partial z} \\
+ (\frac{2x}{R^2}(\frac{\partial R}{\partial z})^2 - \frac{x}{R}\frac{\partial^2 R}{\partial z^2})\frac{\partial C}{\partial x}\}].
\end{aligned} \tag{7.6}$$

## 8. Numerical Method

A finite difference scheme over a uniformly spaced grid is employed to solve the transformed governing equations. All spatial derivatives in Eqs. (7.2) and (7.6) are discretized by central difference approximations, while the time derivatives of $\omega$ and $C$ are discretized by forward difference approximation.

A uniformly spaced grid is generated by introducing the mesh points $(z_i, x_j)$ where $z_i = i\Delta z$ and $x_j = j\Delta x$, where $\Delta z$ and $\Delta x$ are respective increments of $z$ and $x$. The finite difference representation of $t$ is $t_k = k\Delta t$, $\Delta t$ being the time increment.

Corresponding to each line $z = z_i$ in $x$-direction, a tri-diagonal system of algebraic equations is formed. Eq. (7.3) is arranged as

$$A(j)\psi_{i,j-1}^{k+1} + B(j)\psi_{i,j}^{k+1} + C(j)\psi_{i,j+1}^{k+1} = D(j), \tag{8.1}$$

where the quantities $A(j), B(j), C(j)$ and $D(j)$ have following values

$$A(j) = \frac{L_2}{(\Delta x)^2} - \frac{L_1}{2\Delta x}, B(j) = -\frac{2}{(\Delta z)^2} - \frac{2L_2}{(\Delta x)^2}, C(j) = \frac{L_2}{(\Delta x)^2} + \frac{L_1}{2\Delta x}$$

and

$$D(j) = -Rx\omega_{i,j}^k - \frac{\psi_{i+1,j}^k + \psi_{i-1,j}^k}{(\Delta z)^2} + L_3\frac{\psi_{i+1,j+1}^k - \psi_{i+1,j-1}^k - \psi_{i-1,j+1}^k + \psi_{i-1,j-1}^k}{4\Delta z\Delta x}$$

in which

$$L_1 = \frac{2x}{R^2}(\frac{\partial R}{\partial z})^2 - \frac{x}{R}\frac{\partial^2 R}{\partial z^2} - \frac{1}{xR^2}, L_2 = \frac{x^2}{R^2}(\frac{\partial R}{\partial z})^2 + \frac{1}{R^2}, L_3 = \frac{2x}{R}\frac{\partial R}{\partial z}.$$

The well-known Thomas algorithm is now employed to solve the tri-diagonal system of Eqs. (8.1) and we obtain the current value of the stream function. $u$ and $v$ are obtained from Eq. (5.1).

Updated values of the stream function are used to find the wall vorticity as

$$\omega(z, x = 1, t) = -\frac{2}{R^3}[1 + (\frac{\partial R}{\partial z})^2]\frac{\psi_{i,jstp-1} - \psi_{i,jstp}}{(\Delta x)^2} + (\frac{\partial^2 R}{\partial z\partial t} + \frac{1}{R}\frac{\partial R}{\partial z}\frac{\partial R}{\partial t}), \tag{8.2}$$

where $jstp$ represents the value of $j$ at the tube wall.

Same technique is applied to solve the momentum Eq. (7.2). Discretization of the momentum Eq. (7.2) is given by

$$P(j)\omega_{i,j-1}^{k+1} + Q(j)\omega_{i,j}^{k+1} + R(j)\omega_{i,j+1}^{k+1} = S(j), \tag{8.3}$$

where the quantities $P(j), Q(j), R(j)$ and $S(j)$are defined as

$$P(j) = \frac{1}{2\Delta x}(\frac{ux}{R}\frac{\partial R}{\partial z} - \frac{v}{R}) + \frac{1}{Re}(\frac{M_1}{2\Delta x} - \frac{M_2}{(\Delta x)^2}) - M_3 + M_4 + \frac{St}{2\Delta x}\frac{x}{R}\frac{\partial R}{\partial t},$$

$$Q(j) = \frac{St}{\Delta t} - \frac{v}{xR} + \frac{2M_2}{Re(\Delta x)^2} + \frac{\mu}{Re(xR)^2} - \frac{1}{ReR^2x}\frac{\partial \mu}{\partial x},$$

$$R(j) = -\frac{1}{2\Delta x}(\frac{ux}{R}\frac{\partial R}{\partial z} - \frac{v}{R}) - \frac{1}{Re}(\frac{M_1}{2\Delta x} + \frac{M_2}{(\Delta x)^2}) + M_3 - M_4 - \frac{St}{2\Delta x}\frac{x}{R}\frac{\partial R}{\partial t}$$

and

$$S(j) = \frac{St}{\Delta t}\omega_{i,j}^k - u\frac{\omega_{i+1,j}^k - \omega_{i-1,j}^k}{2\Delta z}$$

$$+\frac{\mu}{Re}(\frac{\omega_{i+1,j}^k - 2\omega_{i,j}^k + \omega_{i-1,j}^k}{(\Delta z)^2} - \frac{x}{R}\frac{\partial R}{\partial z}\frac{\omega_{i+1,j+1}^k - \omega_{i+1,j-1}^k - \omega_{i-1,j+1}^k + \omega_{i-1,j-1}^k}{2\Delta z\Delta x})$$

$$+\frac{2}{Re}(\frac{\partial \mu}{\partial z} - \frac{x}{R}\frac{\partial R}{\partial z}\frac{\partial \mu}{\partial x})\frac{\omega_{i+1,j}^k - \omega_{i-1,j}^k}{2\Delta z} + \frac{M}{Re} + \frac{Ha^2}{ReR}\frac{\partial u}{\partial x}$$

in which

$$M_1 = \mu[\frac{2x}{R^2}(\frac{\partial R}{\partial z})^2 - \frac{x}{R}\frac{\partial^2 R}{\partial z^2} + \frac{1}{xR^2}], M_2 = \mu[\frac{x^2}{R^2}(\frac{\partial R}{\partial z})^2 + \frac{1}{R^2}], M_3 = \frac{x}{ReR\Delta x}\frac{\partial R}{\partial z}\frac{\partial \mu}{\partial z},$$

$$M_4 = \frac{1}{ReR^2\Delta x}[x^2(\frac{\partial R}{\partial z})^2 + 1]\frac{\partial \mu}{\partial x},$$

$$M = -\frac{2}{R}(\frac{\partial^2 \mu}{\partial x\partial z} - \frac{1}{R}\frac{\partial R}{\partial z}\frac{\partial \mu}{\partial x} - \frac{x}{R}\frac{\partial R}{\partial z}\frac{\partial^2 \mu}{\partial x^2})(\frac{v}{xR} + 2\frac{\partial u}{\partial z} - \frac{2x}{R}\frac{\partial R}{\partial z}\frac{\partial u}{\partial x})$$

$$+\{\frac{\partial^2\mu}{\partial z^2}+(\frac{x^2}{R^2}(\frac{\partial R}{\partial z})^2-\frac{1}{R^2})\frac{\partial^2\mu}{\partial x^2}-\frac{2x}{R}\frac{\partial R}{\partial z}\frac{\partial^2\mu}{\partial x\partial z}+(\frac{2x}{R^2}(\frac{\partial R}{\partial z})^2-\frac{x}{R}\frac{\partial^2 R}{\partial z^2})\frac{\partial\mu}{\partial x}\}(\frac{1}{R}\frac{\partial u}{\partial x}+\frac{\partial v}{\partial z}-\frac{x}{R}\frac{\partial R}{\partial z}\frac{\partial v}{\partial x}).$$

The mass transport Eq. (7.6) is solved using its discretized version

$$C_{i,j}^{k+1}=C_{i,j}^{k}+\frac{\Delta t}{S t}[N_4\frac{C_{i,j+1}^{k}-C_{i,j-1}^{k}}{2\Delta x}-u\frac{C_{i+1,j}^{k}-C_{i-1,j}^{k}}{2\Delta z}+\frac{1}{ReSc}\{\frac{C_{i+1,j}^{k}-2C_{i,j}^{k}+C_{i-1,j}^{k}}{(\Delta z)^2}$$
$$(-N_3\frac{C_{i+1,j+1}^{k}-C_{i+1,j-1}^{k}-C_{i-1,j+1}^{k}+C_{i-1,j-1}^{k}}{4\Delta z\Delta x}+N_2\frac{C_{i,j+1}^{k}-2C_{i,j}^{k}+C_{i,j-1}^{k}}{(\Delta x)^2}(+N_1\frac{C_{i,j+1}^{k}-C_{i,j-1}^{k}}{2\Delta x}\}], \tag{8.4}$$

where

$$N_1=\frac{2x}{R^2}(\frac{\partial R}{\partial z})^2-\frac{x}{R}\frac{\partial^2 R}{\partial z^2}+\frac{1}{xR^2}, N_2=\frac{x^2}{R^2}(\frac{\partial R}{\partial z})^2+\frac{1}{R^2}, N_3=\frac{2x}{R}\frac{\partial R}{\partial z}, N_4=S t\frac{x}{R}\frac{\partial R}{\partial t}+\frac{ux}{R}\frac{\partial R}{\partial z}-\frac{v}{R}.$$

Once the velocity and concentration field are obtained, the dimensionless wall shear stress and Sherwood number, representing the local mass flux to the arterial wall, are computed by using the formulae

$$WSS=-(\mu\frac{\partial u}{\partial r})_{wall}\ \textbf{and}\ Sh=-2(\frac{\partial C}{\partial r})_{wall}. \tag{8.5}$$

To have a better insight in a pulsatile flow, time-averaged wall shear stress and time-averaged Sherwood number are calculated using the formulae

$$TAWSS=\int_0^1\tau_w dt \text{ and } TASh=\int_0^1 Shdt. \tag{8.6}$$

## 9. Stability Criteria of the numerical scheme

The time step $\Delta t$ is selected through some restrictions on the fluid flow. The first restriction is the well known *CFL* (Courant, Friedrichs & Lewy) condition. It states that the fluid can move through at most one cell in each time step i.e.

$$\Delta t_1\le Min[\frac{\Delta z}{|u|},\frac{\Delta x}{|v|}]_{(i,j)}. \tag{9.1}$$

The viscous effect of the fluid gives the second restriction and is given by

$$\Delta t_2\le Min[\frac{Re}{2}\frac{\Delta z^2\Delta x^2}{\Delta z^2+\Delta x^2}]_{(i,j)}. \tag{9.2}$$

Finally, $\Delta t$ is calculated by the relation

$$\Delta t=\beta Min[\Delta t_1,\Delta t_2], 0<\beta<1. \tag{9.3}$$

## 10. Results and Discussion

Present mathematical model is employed for a detailed quantitative analysis to study the distribution of wall shear stress and mass transfer phenomenon in *MHD* flow of blood. Qualitative similarity of obtained results with existing and available literature confirms the applicability of present model.

It is well established that the initiation and development of arterial diseases are closely associated with the distribution of wall shear stress. Higher magnitudes of wall shear stress may damage the vessel wall. On the contrary, excess fatty substances, borne by the blood stream, get an opportunity to be deposited on the inner wall of an artery in the regions of low wall shear stress and this propagates atherosclerosis. Thus investigation of the distribution of wall shear stress at the stenotic and post-stenotic region deserves special attention.

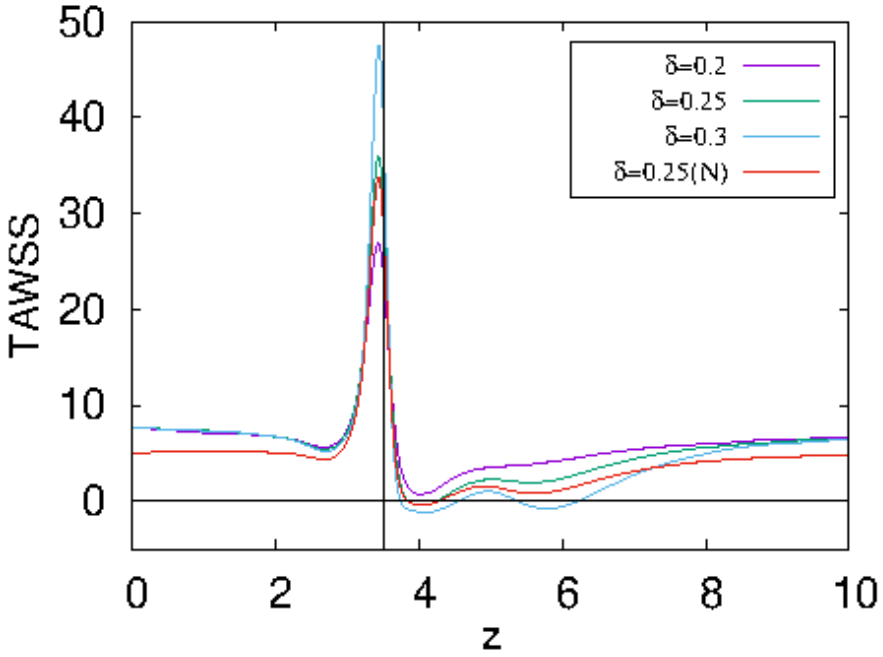


***Fig*. 10.1(a)**

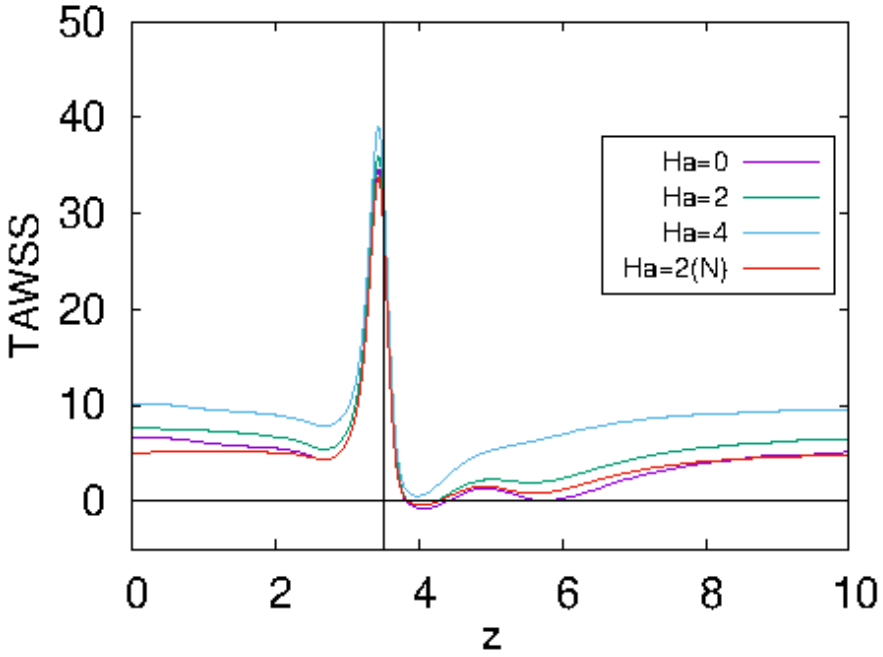


***Fig*. 10.1(b)**

***Fig*. 10.1**. Distributions of time-averaged wall shear stress for different **(a)** constriction heights and $Ha = 2$; **(b)** Hartmann numbers and $\delta = 0.25$.

Distributions of time-averaged wall shear stress for variations of $\delta$ and $Ha$ are presented in *Figs*. 10.1(a) and 10.1(b). Time-averaged wall shear stress rises considerably in the stenotic zone and attains its maximum slightly

upstream of the throat (the vertical line indicates the position of stenosis throat). In some region of the downstream side of the stenosis, wall shear stress becomes negative. This negative value indicates the flow separation zone. Flow separation changes the flow structure, forms vortex and the separation length gives an idea about the size of vortex. Formation of recirculation zone is of pathological significance, since this region prolongs the residing time of blood constituents which may eventually be put down onto the arterial wall and forms secondary stenosis.

One may note that the peak $TAWSS$ and the time-averaged length of separation increases with severity of constriction. For $\delta = 0.3$ (51% area reduction), two separation zones are noticed. Increasing magnetic field increases the peak $TAWSS$ but reduces the separation length. Peak value of $TAWSS$ increases, but the time-averaged length of separation decreases in case of non-Newtonian fluid compared to Newtonian fluid (*Fig*. 10.1(a)).

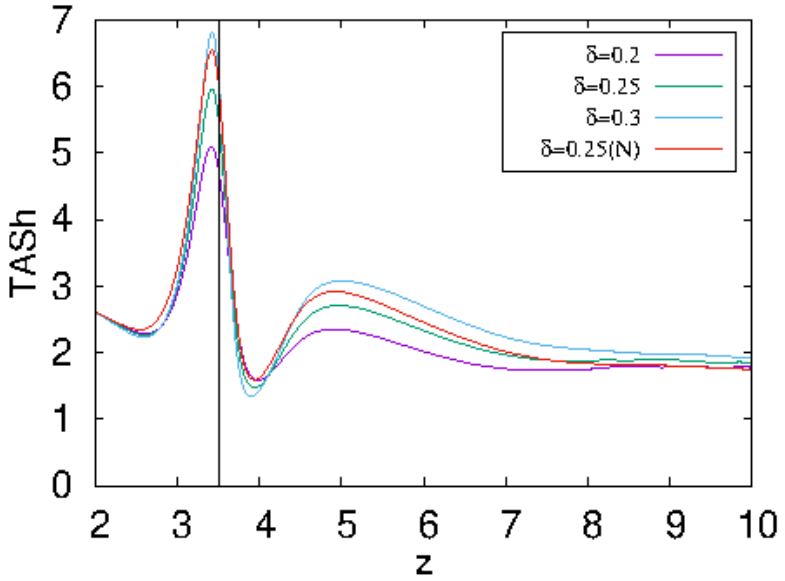


***Fig*. 10.2(a)**

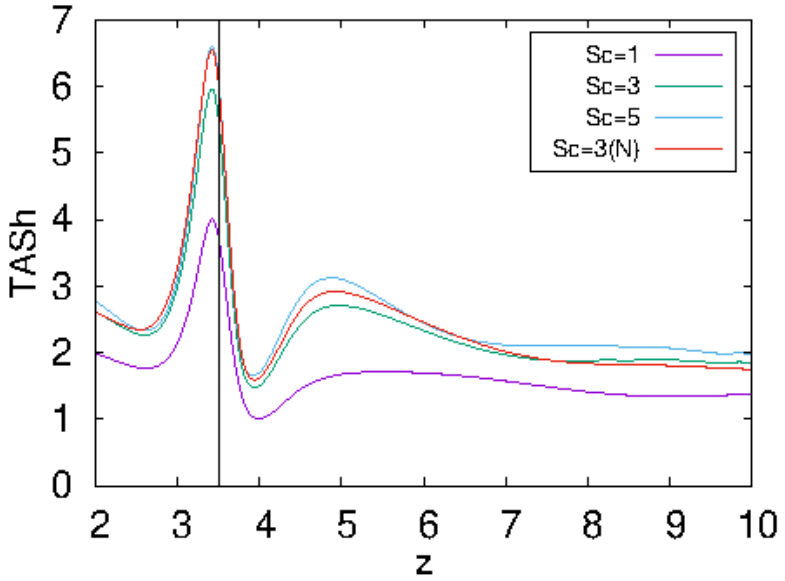


***Fig*. 10.2(b)**

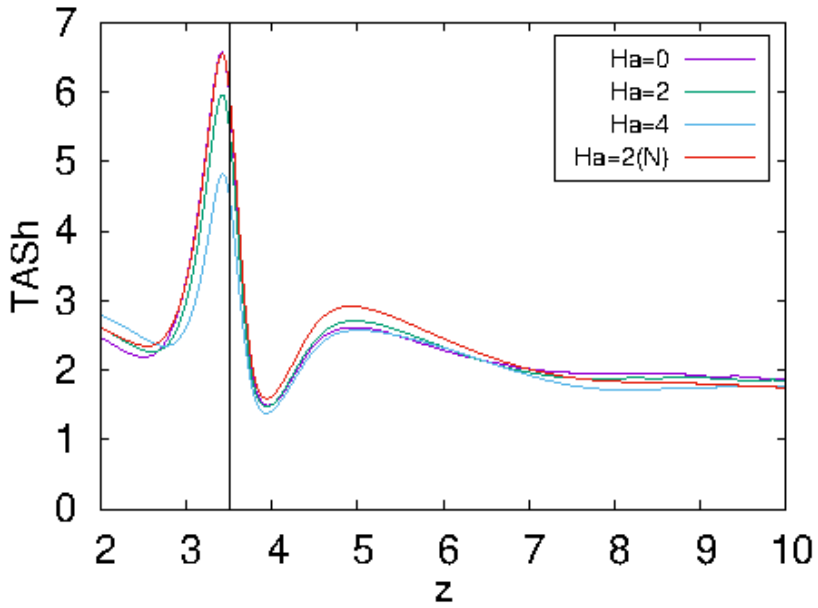


***Fig*. 10.2(c)**

***Fig*. 10.2.** Distributions of time-averaged Sherwood number for different **(a)** constriction heights and $Ha = 2, Sc = 3$; **(b)** Schmidt numbers and $\delta = 0.25, Ha = 2$; **(c)** Hartmann numbers and $\delta = 0.25, Sc = 3$.

Mass flux from the blood stream onto the arterial wall is measured with the help of the Sherwood number. Distributions of the time-averaged Sherwood number over the entire flow regime under consideration are computed for several of $\delta, Ha$ and $Sc$ and are presented in *Figs.* 10.2(a) to 10.2(c). Maximum mass transfer rate is noted slightly upstream of the stenosis throat in all cases like the time-averaged wall shear stress. This result was also obtained by earlier researchers like Kaazempur-Mofrad et al. [10] and Sarifuddin et al. [23]. In the lee of the constriction another prominent peak is noted. Thus the mass transfer rate again rises just behind the stenosis. This phenomenon could explain the development of secondary stenosis which is observed in clinical practice [5] with the enlargement of existing one.

Mass transfer rate over the entire flow regime increases with the degree of stenosis (*Fig*. 10.2(a)). Thus advancement of the disease further deteriorates the health condition of arterial wall and the disease propagates. Increasing Schmidt number also increases the mass transfer rate (*Fig*. 10.2(b)). Increasing strength of magnetic field, however, reduces the mass transfer rate at the arterial wall. Applied magnetic field affects the velocity field of the moving fluid, which, in turn, slowed down the mass transfer rate ( *Fig*. 10.2(c)). Mass transfer phenomenon takes place less in case of non-Newtonian fluid compared to that of Newtonian fluid. Lower viscosity of Newtonian fluid is responsible for greater rate of mass transfer.

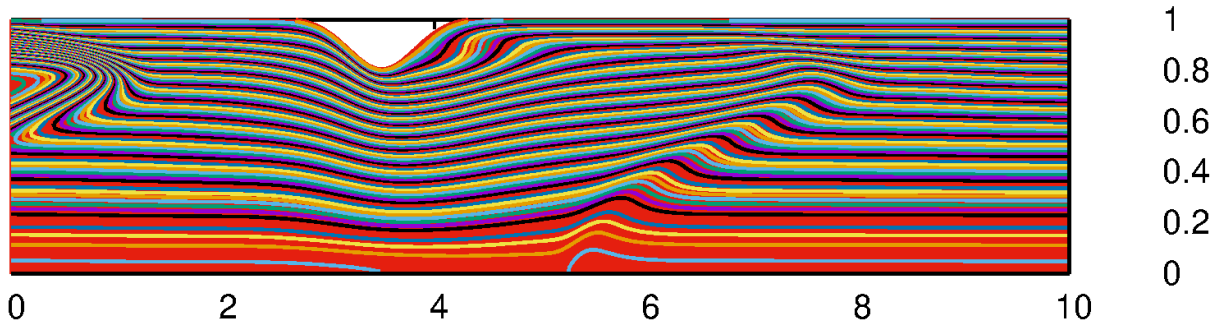


**(a)**

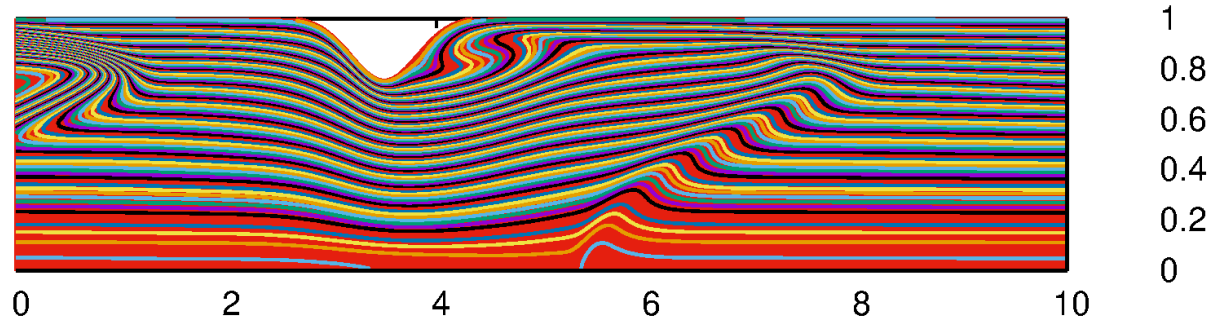


**(b)**

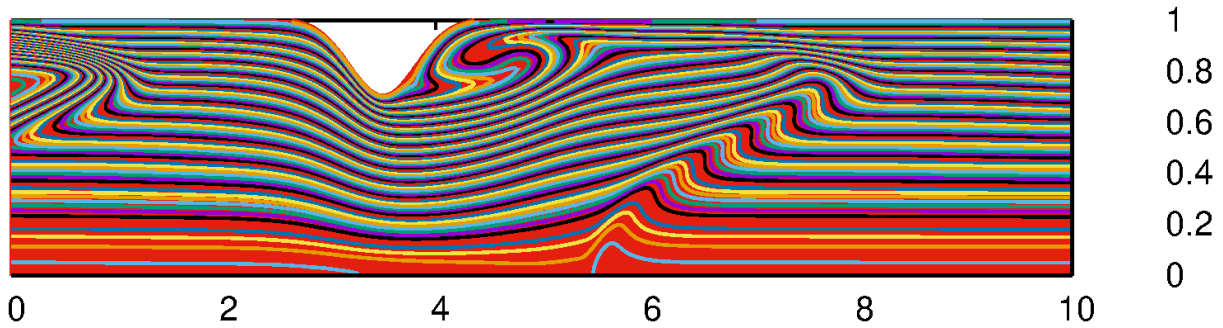


**(c)**

***Figure* 10.3:** Patterns of iso-concentration lines at $t = 0.18$ for $Ha = 2$ and **(a)** $\delta = 0.2$; **(b)** $\delta = 0.25$; **(c)** $\delta = 0.3$

Patterns of iso-concentration lines describe the concentration field very nicely. *Figs.* 10.3(a) to 10.3(c) are prepared to depict the concentration field for various constriction heights. Formation of a stenosis disturbs the normal flow of blood. This flow disturbance causes the iso-concentration lines to be intense in the stenotic and post-stenotic region. Thus the concentration gradient and hence the mass transfer rate along the arterial wall rises up significantly in these regions.

## 11. Conclusions

Normal arterial flow becomes perturbed by the initiation of atherosclerosis and the changed hemodynamic environment propagates the disease. Mathematical modeling and numerical simulation of arterial flow is helpful to explore possible causes and effects of such arterial disease. Major findings of this numerical study are as follows:

1. Blood flow becomes more instable in the stenotic and post stenotic regions.
2. Wall shear stress rises considerably in the stenotic region and gains its peak value slightly upstream of the stenosis throat. Flow separation takes place in the rear side of the constriction.
3. Applied magnetic field increases the wall shear stress but reduces the separation length.
4. Formation of a mild stenosis further helps to propagate the disease.

5. Externally imposed magnetic field can delayed the development of atherosclerosis.

**Acknowledgement.** Thanks are indeed due to the respected editors and reviewers of this Journal for their constructive suggestions for the improvement of the paper. The author is also grateful to Prof. Swati Mukhopadhyay, The University of Burdwan for her continuous encouragement to carry out this research work.

**References**

[1] L. H. Back, J. R. Radbill and D. W. Crawford, Analysis of oxygen transport from pulsatile viscous blood flow to diseased coronary arteries of man, *J. Biomech.*, **10** (1977), 763-774.

[2] C. G. Caro, J. M. Fitz-Gerald and R. C. Schroter, Proposal of a shear dependent mass transfer mechanism for atherogenesis, *Clin. Sci.*, **40** (1971), p.5.

[3] S. E. Charm and G. Kurland, Viscometry of human blood for shear rates 0-100,000 $\sec^{-1}$, *Nature*, **206** (1965), 617-618.

[4] Y. I. Cho and K. R. Kensey, Effects of the non-Newtonian viscosity of blood on flows in a diseased arterial vessel. Part I: Steady flows, *Biorheology*, **28** (1991), 241-262.

[5] M. E. DeBakey, G. M. Lawrie and D. H. Glaeser, Patterns of atherosclerosis and their surgical significance, *Ann. Surg.*, **201** (1985), 115-131.

[6] C. R. Etheir, Computational modeling of mass transfer and links to atherosclerosis, *Ann. Biomed. Eng.*, **30** (2002), 461-471.

[7] Y. Haik, V. Pai and C. J. Chen, Development of magnetic device for cell separation, *J. Magn. Magn. Mater.*, **194** (1999), 254-261.

[8] C. E. Huckaba and A. N. Hahn, A generalized approach to the modelling of arterial blood flow, *Bull. Math. Biophys.*, **30** (1968), 645-662.

[9] M. Jahangiri, M. Saghafian and M. R. Sadeghi, Numerical simulation of non-Newtonian models effect on hemodynamic factors of pulsatile blood flow in elastic stenosed artery, *J. Mech. Sci. Tech.*, **31**(2) (2017), 1003-1013.

[10] M. R. Kaazempur-Mofrad, S. Wada, J. G. Myers and C. R. Ethier, Mass transfer and fluid flow in stenotic arteries: Axisymmetric and asymmetric models, *Int. J. Heat and Mass Transfer*, **48** (2005), 4510-4517.

[11] D. N. Ku, D. P. Giddens, C. K. Zarins and S. Glagov, Pulsatile flow and atherosclerosis in the human carotid bifurcation: positive correlation between plaque location and low and oscillating shear stress, *Atherosclerosis,* **5** (1985), 293-302.

[12] S. C. Ling and H. B. Atabek, A nonlinear analysis of pulsatile flow in arteries, *J. Fluid Mech.*, 55 (1972), 493-511.

[13] P. Ma, X. Li and D. N. Ku, Heat and mass transfer in a separated flow region for high Prandtl and Schmidt numbers under pulsatile conditions, *Int. J. Heat and Mass Transfer*, **37** (1994), 2723-2736.

[14] M. S. Mandal, S. Mukhopadhyay and G. C. Layek, Pulsatile flow of shear-dependent fluid in a stenosed artery, *Theoret. Appl. Mech.*, **39** (2012), 209-231.

[15] J. C. Misra, A. Sinha and G. C. Shit, Flow of a biomagnetic viscoelastic fluid: application to estimation of blood flow in arteries during electromagnetic hyperthermia, a therapeutic procedure for cancer treatment, *Appl. Math. Mech.*, **31**(11) (2010), 1405-1420.

[16] S. Mukhopadhyay, M. S. Mandal and S. Mukhopadhyay, Numerical simulation of physiologically relevant pulsatile flow of blood with shear-rate-dependent viscosity in a stenosed blood vessel, *Int. J. Biomath.,* **11**(6) (2018), 1-22.

[17] S. Mukhopadhyay, M. S. Mandal and S. Mukhopadhyay, Numerical investigation of mass transfer in pulsatile flow of blood characterized by Carreau model under stenotic condition, *J. Appl. Fluid. Mech.*, **14**(3) (2021), 805-817.

[18] M. Nakamura and T. Sawada, Numerical study on the unsteady flow of non-Newtonian fluid, *J. Biomech. Engg.*, **112** (1990),100-103.

[19] N. Nandakumar, K. C. Sahu and M. Anand, Pulsatile flow of a shear-thinning model for blood through a two dimensional stenosed channel, *Eur. J. Mech. B/Fluids*, **49** (2015), 29-35.

[20] G. Pedrizzetti, Unsteady tube flow over an expansion, *J. Fluid Mech.*, **310** (1996), 89-111.

[21] G. Pontrelli, Blood flow through an axisymmetric stenosis, *Proc. Instn. Mech. Engrs.*, **215** (2001), 1-10.

[22] G. Rappitsch, K. Perktold and E. Pernkopf, Numerical modelling of shear-dependent mass transfer in large arteries, *Int. J. Numer. Methods in Fluids*, **25** (1997), 847-857.

[23] Sarifuddin, S. Chakravarty, P. K. Mandal and H. I. Anderson, Mass Transfer to blood flowing through arterial stenosis, *Z. angew. Math. Phys.*, **60** (2009), 299-323.

[24] G. C. Shit and S. Majee, Magnetic field interaction with blood flow and heat transfer through diseased artery having Abdominal Aortic *Aneurysm, Eur. J. Mech. B/ Fluids*, **71** (2018), 1-14.
[25] J. V. Soulis, G. D. Giannoglou, Y. S. Chatzizisis, K. V. Seralidou, G. E. Parcharidis and G. E. Louridas, Non-Newtonian models for molecular viscosity and wall shear stress in a 3D reconstructed human left coronary artery, *Med. Engg. Phy.*, 30 (2008), 9-19.
[26] . Trk, M. Tezer-Sezgin and C. Bozkaya, Finite element study of biomagnetic fluid flow in a symmetrically stenosed channel, *J. Comput. Appl. Math.*, **259** (2014), 760-770.
[27] E. E. Tzirtzilakis, Biomagnetic fluid flow in a channel with stenosis, *Physica D*, **237** (2008), 66-81.
[28] P. A. Voltairas, D. I. Fotiadis and L. K. Michalis, Hydrodynamics of magnetic drug targeting, *J. Biomech.*, **35** (2002), 813-821.
[29] R. L. Whitmore, Rheology of the circulation, Pergamon Press, New York, 1968.
[30] A. Zaman, N. Ali, O. A. Bg and M. Sajid, Heat and mass transfer to blood flowing through a tapered overlapping stenosed artery, *Int. J. Heat and Mass Transfer*, **95** (2016), 1084-1095.